Journal of Geodesy (2019) 93:1501–1514
https://doi.org/10.1007/s00190-019-01263-9

ORIGINAL ARTICLE

Assessment of forecast Vienna Mapping Function 1 for real-time tropospheric delay modeling in GNSS

Yubin Yuan[1] · Lucas Holden[1] · Allison Kealy[1] · Suelynn Choy[1] · Paweł Hordyniec[1,2]

Received: 14 August 2018 / Accepted: 12 May 2019 / Published online: 23 May 2019

Abstract
The accurate modeling of tropospheric path delay is significant for data processing of radio space-geodetic techniques such as Global Navigation Satellite System (GNSS) and Very-Long-Baseline Interferometry (VLBI). The Vienna Mapping Function 1 (VMF1) model, based on continuous update of Numerical Weather Prediction (NWP) data from the European Centre for Medium-Range Weather Forecasts (ECMWF), is recommended for this purpose in post-processing. The VMF1 coefficients determined from forecast data of the ECMWF are now readily and freely available. However, little or no implementation of this forecast VMF1 (VMF1-FC) model in real-time GNSS or VLBI applications has occurred. This study investigates the performance of the VMF1-FC model in terms of its three components which are critical for the modeling of tropospheric path delay: the Zenith Hydrostatic Delay (ZHD), the Zenith Wet Delay (ZWD) and mapping functions. All three components are assessed in the context of GNSS Precise Point Positioning (PPP) using 28 global stations over a 70-day period. The Zenith Total Delays (ZTD) derived with the VMF1-FC (implemented in real-time PPP) are shown to agree well with the tropospheric delay product from the Center for Orbit Determination Europe (CODE). Root mean square (RMS) errors associated with these ZTD estimates are < 10 mm at all 28 stations. The results also show that the VMF1-FC model performs better than empirical models such as the widely used Global Pressure and Temperature 2 (GPT2) and GPT2 wet (GPT2w), with smaller RMS errors associated with the ZTD estimates. It is recommended that VMF1-FC be applied for future tropospheric delay modeling in real-time GNSS and VLBI applications.

Keywords Precise Point Positioning · Vienna Mapping Function · Tropospheric delay · Zenith Total Delay · Zenith Wet Delay · GNSS meteorology

1 Introduction

Tropospheric path delay is a major error source in Global Navigation Satellite System (GNSS) and Very-Long-Baseline Interferometry (VLBI) data processing. Mitigation of this error is essential to obtain high-precision positioning results for geodetic applications. In the GNSS analysis, the tropospheric path delay is typically estimated and can then be used to retrieve precipitable water vapor (PWV) (Bevis et al. 1992; Tregoning et al. 1998). Tropospheric path delay is typically accounted for using the sum of hydrostatic and wet parts. Both are mapped into the zenith directions, i.e., Zenith Hydrostatic Delay (ZHD) and Zenith Wet Delay (ZWD), using the following equation:

$$D_{\text{trop}} = \text{ZHD} \cdot mf_{\text{h}} + \text{ZWD} \cdot mf_{\text{w}} \tag{1}$$

where mf_{h} and mf_{w} represent the hydrostatic and wet mapping functions. In Eq. (1), efforts can be made to improve the a priori ZHD, ZWD and/or mapping functions to better refine the modeling of tropospheric delay. If the surface pressure P is known, the ZHD can be accurately modeled using the following empirical function:

$$\text{ZHD} = 0.0022768P/(1 - 0.00266\cos(2\varphi) - 0.28 \times 10^{-6}h) \tag{2}$$

where φ and h represent station latitude and height, respectively (Davis et al. 1985).

The surface pressure may be measured by in situ barometers and stored in the Receiver Independent Exchange

✉ Yubin Yuan
yubin.yuan@rmit.edu.au

[1] School of Science, RMIT University, GPO Box 2476, Melbourne, VIC 3001, Australia

[2] Institute of Geodesy and Geoinformatics, Wrocław University of Environmental and Life Sciences, Grunwaldzka 53, 50-375 Wroclaw, Poland

Format (RINEX), or obtained from Numerical Weather Prediction (NWP) datasets. In both instances, the positioning accuracies, particularly, that of the height component, are improved significantly (Fund et al. 2011). Unfortunately, ZWD is more difficult to determine due to high variability of atmospheric water vapor distributions. In this case, an extra parameter is typically used, either using piecewise linear interpolation or random walk process, to account for this variability (Kouba and Heroux 2001). The introduced parameter can be either the ZWD itself, or a correction to an a priori value such as provided by NWP models (Bevis et al. 1996).

Conventionally, mapping functions are determined using Eq. (3) (Herring 1992; Marini 1972; Niell 1996), with three coefficients a, b and c, for a given elevation angle e.

$$mf(e) = \frac{1 + \frac{a}{1+\frac{b}{1+c}}}{\sin(e) + \frac{a}{\sin(e)+\frac{b}{\sin(e)+c}}} \tag{3}$$

In Eq. (3), the three coefficients for a hydrostatic mapping function (ah, bh, ch) are different from those for a wet mapping function (aw, bw, cw). Based on this equation, the Vienna University of Technology developed the VMF1 (Vienna Mapping Function 1) model (Boehm et al. 2006b) and the empirical GPT/GMF (Global Pressure and Temperature/Global Mapping Function) model (Boehm et al. 2006a, 2007). These models provide not only mapping functions, but also a priori ZHD and ZWD, and have been widely used in GNSS and VLBI data processing and applications.

The GPT/GMF model was later upgraded to GPT2 (Lagler et al. 2013) which provides pressure, temperature, mapping function coefficients (ah, aw, bh, bw, ch and cw), temperature lapse rate and water vapor pressure on a global $5° \times 5°$ grid. ZHD can then be computed using surface pressure and Eq. (2), while hydrostatic and wet mapping functions can be computed using Eq. (3). GPT2 wet (GPT2w) (Boehm et al. 2015) is upgraded from GPT2, also providing ZWD which may not only be used for positioning and navigation purposes, but also for other high-precision applications.

The VMF1 coefficients ZHD, ZWD, ah and aw are continuously updated on a daily basis using NWP model data from the European Centre for Medium-Range Weather Forecasts (ECMWF). Incorporating such VMF1 coefficients is recommended in high-precision GNSS data processing by the latest IERS conventions (Petit and Luzum 2010). These coefficients are provided on a global grid ($2.5° \times 2.0°$) as well as at the selected stations of international GNSS service (IGS), international VLBI service (IVS) and international Doppler orbitography and radio positioning integrated by satellite service (IDS). The VMF1 coefficients determined from forecast data of the ECMWF were also made available (Boehm et al. 2009). In this research, three types of VMF1 datasets, the post-processed site-specific VMF1 (termed here as VMF1-site), the post-processed gridded VMF1 (termed here as VMF1-grid) and forecast gridded VMF1 (termed here as VMF1-FC), are implemented and compared.

Boehm et al. (2009) analyzed the accuracies of the parameters derived from the VMF1-FC dataset. Their simulation results showed that the station height differences using VMF1-grid and VMF1-FC coefficients were below 1 mm. However, to date, not much implementation of this forecast VMF1 model has been performed in real-time GNSS or VLBI applications. This is because high-precision real-time Precise Point Positioning (PPP) (Zumberge et al. 1997) has only recently become possible with the release of the real-time products by the IGS (Agrotis et al. 2012). Wilgan et al. (2017) investigated the possibility of applying NWP model data to account for the tropospheric delay in real-time PPP. They concluded that the a priori ZHD derived from the near-real-time GNSS data and NWP model resulted in an average reduction of 3D bias but an increase of 3D standard deviation at the selected 14 stations in Poland.

In this research, the VMF1-FC dataset is validated in the context of real-time retrieval of Zenith Total Delays (ZTD) using the Precise Point Positioning (PPP) technique. The retrieved ZTDs are compared to the tropospheric products from the Center for Orbit Determination in Europe (CODE) for validation (from http://ftp.aiub.unibe.ch/CODE/2016/). CODE provides reliable ZTD products for IGS stations at 2-h intervals with a latency of 2 weeks over approximately 250 globally distributed stations (Dach et al. 2009). Their GNSS data are post-processed with a cutoff angle 3° on the Bernese software, but with a relative positioning technique. The GPT/GMF model is used for the modeling of tropospheric delay.

Twenty-eight globally distributed IGS stations over a randomly selected 70-day period (June 15 to August 24, 2016, see Fig. 1) are selected for the testing. This includes all IGS stations that have CODE ZTD products and in situ meteorological observations in the RINEX format. The latter is essential to properly assess the performance of the a priori ZHD from VMF1-FC. The GPS and GLONASS observations are processed every 30 s using the BKG Ntrip Client (BNC) (Mervart and Weber 2013) which has been modified by Yuan et al. (2014) to provide high-precision PPP solutions. The low elevation observations are essential to decorrelate the estimated station height and the tropospheric delay parameter; hence, a cutoff angle 5° is set in PPP. However, the observations with elevation angles $< 20°$ are down weighted using a coefficient $1.5–0.5 \times (\text{ele}-10.0)/(20.0-10.0)$, which is used by default in BNC. We assume that the uncertainties of the initial Easting/Northing, Height

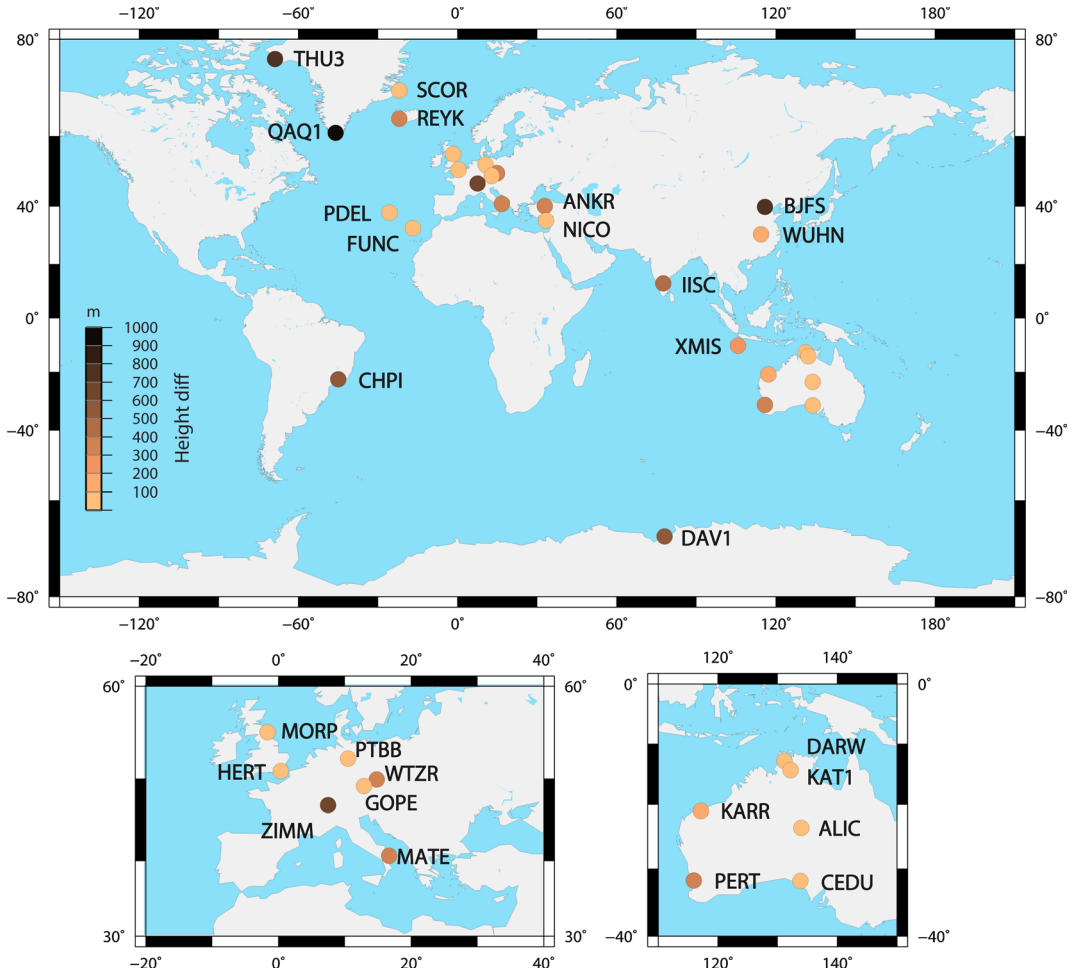

Fig. 1 Location of the selected 28 stations used in this research. The color at each station represents the ellipsoidal height difference between the station height h_s and the mean grid height h_g. h_g is calculated using the four surrounding grid points for the determination of VMF1-FC coefficients

and ZTD are 2 m, 2 m and 0.05 m, respectively. This is reasonable as we use the coordinates from the IGS log files. As for the noises, for an observation interval of 30 s, we assume changes of 0.3 mm in Easting and Northing and 0.6 mm in Height and 0.3 mm in the ZWD parameter. All these noise level values are tested and found to work well in the context of ZTD retrieval in this research.

2 Determination of VMF1-FC coefficients for real-time applications

The VMF1-FC dataset is predicted and routinely updated every day at about 8 Universal Time (UT). In each update, four files with respect to epochs 0, 6, 12, 18 UT for the following day are provided. To obtain the tropospheric delay parameters for the current epoch, an interpolation using the latest several VMF1-FC files is needed, e.g., using a cubic spline or Lagrange interpolation within a sliding window of eight consecutive VMF1-FC files. This optimizes the quality of the forecast information and ensures no major offsets in the interpolated parameters. This interpolation can then be followed by another spatial interpolation to the specified geographic location defined by latitude and longitude using the four surrounding grid points. The mean grid height is also calculated in this process. Bilinear interpolation using station latitude and longitude, as presented in (Yuan 2015), is ideal for this purpose.

In this process, the station height h_s and the calculated mean grid height h_g will not be identical, with some height differences greater than 1000 meters (e.g., stations BJFS, CHPI, DAV1, QAQ1 and ZIMM in Fig. 1). Therefore, height corrections must be applied when coefficients *ah*, *aw*, ZHD and ZWD are interpolated and used in PPP processing.

To calculate these corrections, surface pressure P_s must first be determined from the interpolated P_g which is based on the mean grid height h_g. According to (Boehm et al. 2007), this can be achieved using Eq. (4):

$$P_s = P_g(1 - 0.0000226(h_s - h_g))^{5.225} \tag{4}$$

where P_s can then be used as an input to Eq. (2) to determine the ZHD.

The coefficients *ah* and *aw* derived using the VMF1-site dataset are valid for the actual ellipsoid height of the station. However, those derived using the VMF1-FC dataset are valid for zero height; hence, height corrections are needed to reduce them to the station ellipsoidal height. The height correction for coefficient *ah* can be applied by adding h_{corr} to the hydrostatic mapping function (Eq. (5)) (Niell 1996).

$$h_{corr} = \left(\frac{1}{\sin(e)} - \frac{1 + \frac{a_0}{\left(1 + \frac{b_0}{(1+c_0)}\right)}}{\sin(e) + \frac{a_0}{\sin(e) + \frac{b_0}{\sin(e)+c_0}}} \right) \cdot \frac{h_s}{1000} \tag{5}$$

where $a_0 = 2.53 \times 10^{-5}, b_0 = 5.49 \times 10^{-3}, c_0 = 1.14 \times 10^{-3}$ are empirical values.

Unfortunately, no straightforward transformations are readily available for coefficients *aw* and ZWD. However, Kouba (2008) suggests that a linear decay function for coefficient *aw* could be used in this context. This function is Eq. (6):

$$aw_s = aw_0 + k_{aw}(h_s - h_0) \quad (h_0 = 0) \tag{6}$$

where k_{aw} is the linear decay coefficient. If coefficient aw_s at the station height and aw_0 at zero height are available during one specific period, coefficient k_{aw} can then be determined using a linear regression approach. The linear correlation between aw_s and aw_0 can also be simplified as $y = ax + b$. To obtain these linear regression coefficients, aw_s derived from the VMF1-site dataset and aw_0 derived from the VMF1-grid dataset can be used, which is the case in this research.

Kouba (2008) also suggested that an exponential decay function [Eq. (7)] with coefficient k_{ZWD} is ideal for the reduction of ZWD to the station height:

$$ZWD_s = ZWD_g \cdot e^{k_{ZWD}(h_s - h_g)} \tag{7}$$

Moreover, Dousa and Elias (2014) demonstrated that the exponential decay of ZWD could also be expressed as

$$ZWD_s = \left(\frac{P_s}{P_g}\right)^{\lambda+1} ZWD_g \tag{8}$$

where λ represents the vertical decay ratio. According to Eqs. (7) and (8), if the parameters h_g, P_g, ZWD_g derived from the VMF1-grid dataset and the parameters h_s, P_s, ZWD_s derived from the VMF1-site are known, a linear regression approach and its determined coefficients can also be used to reduce ZWD to the station height. The reduction process is similar to that of coefficient *aw*. In this research, the VMF1-grid and VMF1-site datasets during 2016 are used to determine the linear regression coefficients for *aw* and ZWD.

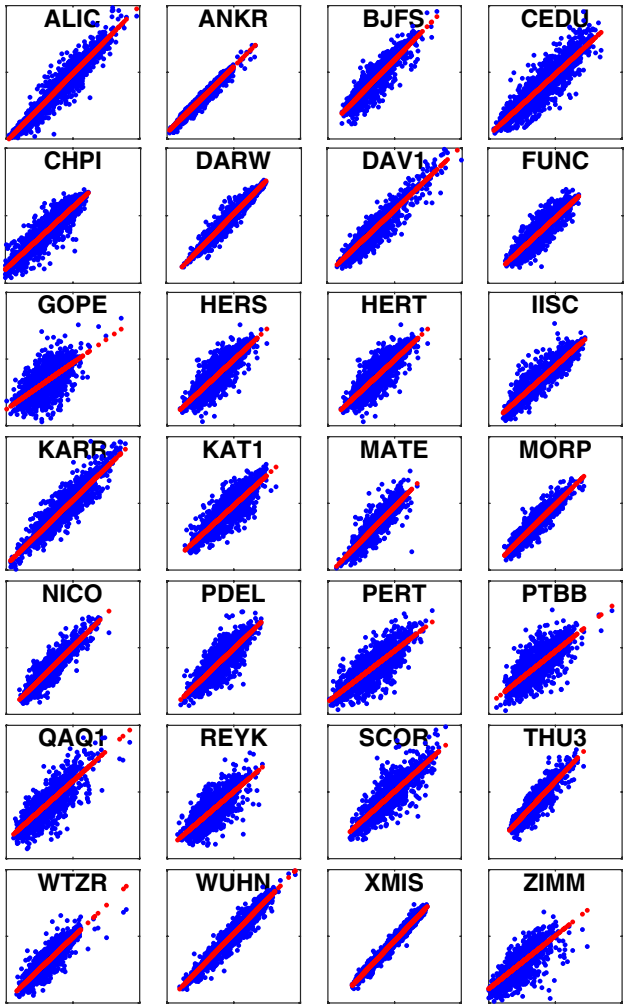

Fig. 2 Linear regression in the form of $y = a + bx$ for coefficient *aw*. The horizontal axis represents values at zero height derived from the VMF1-grid dataset, while the vertical axis represents the values at station height derived from the VMF1-site dataset. Both axes range between 4e−4 and 8e−4. Both datasets cover a 1-year period between June 2015 and June 2016

Figures 2 and 3 show how linear regression works for coefficients *aw* and ZWD. For each subfigure, the regression slope indicates the strength of the linear relationship between the VMF1-grid and VMF1-site datasets. One can see that at most of the stations, the two datasets are highly correlated. This indicates that linear regression is appropriate to reduce the calculated *aw* and ZWD from the VMF1-FC dataset to station height. However, this may not include stations CEDU, CHPI, GOPE, KAT1. Such stations are either with complex terrain (i.e., height differences between GNSS station and grid points are large), or in an area where spatial and temporal variation of water vapor is substantial;

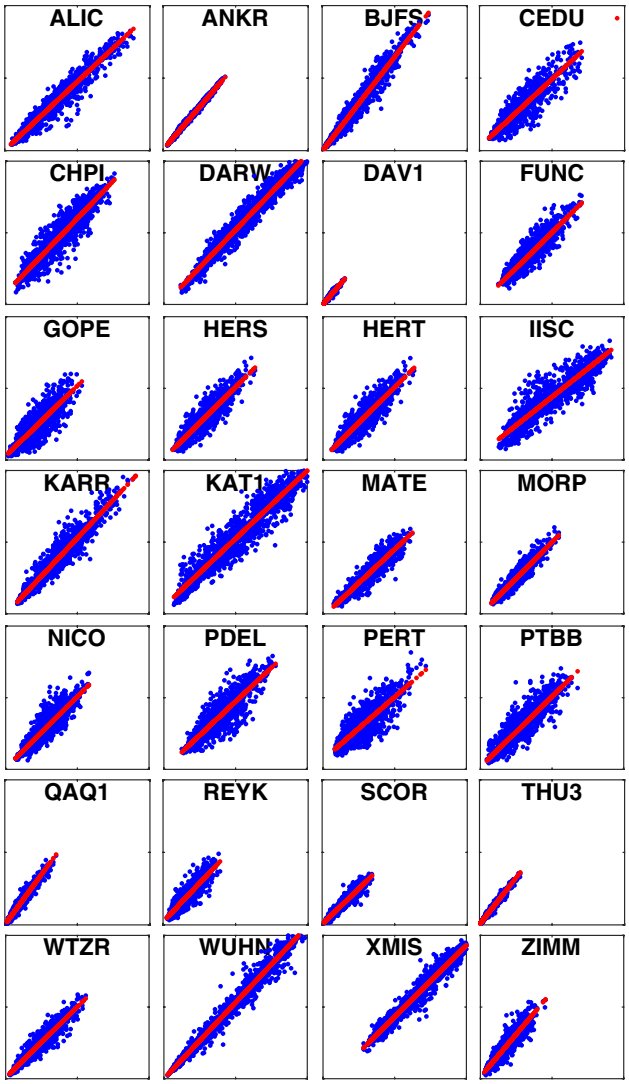

Fig. 3 Linear regression in the form of $y=a+bx$ for coefficient ZWD. The horizontal axis represents values at mean grid height derived from the VMF1-grid dataset, while the vertical axis represents the values at station height derived from the VMF1-site dataset. Both axes range between 0 and 0.4 m. Both datasets cover a 1-year period between June 2015 and June 2016

hence, ZWD is difficult to predict. We will compare the post-processed results with and without height corrections implemented in PPP in next three sections.

3 Performance of VMF1-FC mapping functions

Three scenarios are used to assess the performance of the VMF1-FC ZHD, ZWD and mapping functions, respectively. In the first scenario, the a priori ZHD coefficients derived from in situ surface pressure observations are held constant while different mapping functions are used in real-time PPP. The root mean square (RMS) error, which is based on the differences to reference CODE ZTD products, is used for validation.

The results show that the RMS errors of the ZTD estimates derived from the VMF1-FC dataset (in Table 1) are much smaller than those derived from the Niell Mapping Function (NMF) (Niell 1996) and the GPT2 model. This suggests that the VMF1-FC dataset is superior to the NMF and GPT2 models particularly for the polar stations, i.e., DAV1, QAQ1 and THU3. The improvement is due to continuous updates of VMF1-FC coefficients using ECMWF data, as opposed to NMF and GPT2 empirical models. Currently, the GPT2 model is widely used in real-time GNSS applications. An improvement is expected if the VMF1-FC mapping functions are used instead. Table 1 also indicates that the solutions based on the VMF1-FC dataset are very similar to those of the VMF1-grid, although the latter is post-processed and deemed to be better than the forecast model.

Table 1 shows that the RMS errors at these 28 stations range from 3.0 mm to 10.1 mm, with an average value of 6.6 mm at all stations. A further investigation shows that the mean biases of ZTDs to the reference ZTD products are close to zero at each station. The RMS errors are likely caused by the variations of the PPP ZTDs. In particular, when the temporal variation of ZTDs is very high, the difference between the PPP ZTD and CODE ZTD can be up to 25.4 mm at station ALIC (see Fig. 4). This is because we fix the noise level of ZTD in PPP, i.e., assuming a ZTD change of 0.3 mm during 30 s. In moderate weather conditions, this assumption works well. However, it is not sufficiently enough to capture high variation signals of ZTD. Another factor that causes ZTD outliers is internet outage, which makes retrieval of IGS real-time corrections unavailable. If the outage is minor, the variance–covariance matrix in the Kalman filtering is kept and still works for the new epoch after the internet connection is regained. However, if it is a major outage, the variance–covariance matrix is useless for the new epoch; hence, BNC needs to re-initialize the processing. In this case, the PPP results in the first hour after the internet connection is regained are excluded for ZTD comparisons. Both minor and major internet outages at station WUHN, as well as their effects on the ZTD retrievals, are shown in Fig. 4.

A comparison between the results using the VMF1-FC dataset, with and without a height correction to coefficient *aw* (VMF1-FC2 and VMF1-FC1 in Table 1, respectively), shows very minor RMS error differences. Therefore, it is difficult to determine which solution is more accurate. Zus et al. (2015) analyzed the systematic errors of VMF1 mapping functions on a global scale. They concluded that a mapping function which is based on the VMF1 concept did have systematic errors because it is tuned for specific

Table 1 RMS errors of ZTDs using reference ZTD products from CODE. The a priori ZHD derived from in situ meteorological data is held constant, while different mapping functions are used in PPP. Columns 3–8 show the differences to VMF1-FC1 solutions, and a positive value indicates that the corresponding RMS error is larger than its VMF1-FC1 counterpart

Station	VMF1-FC1[a] (RMS:mm)	VMF1-FC2[b] (Δ:mm)	VMF1-grid1[a] (Δ:mm)	VMF1-grid2[b] (Δ:mm)	NMF (Δ:mm)	GPT2 (Δ:mm)	GPT2w (Δ:mm)
ALIC	4.8	−0.1	−0.1	−0.1	−0.1	−0.1	−0.1
ANKR	5.5	0	+0.1	+0.1	+0.3	+0.3	+0.3
BJFS	5.7	−0.1	−0.1	−0.1	0	−0.2	−0.2
CEDU	7.3	0	0	0	+7.9	−0.3	−0.3
CHPI	6.1	−0.1	0	−0.1	0	0	0
DARW	5.6	0	0	0	+89.7	0	0
DAV1	3.0	+0.1	0	0	+11.4	+1.0	+1.2
FUNC	6.3	0	0	0	+0.2	+0.1	+0.1
GOPE	7.1	0	−0.1	−0.1	+0.3	+0.2	+0.2
HERS	6.2	0	0	0	+0.3	+0.6	+0.6
HERT	8.2	0	0	0	+0.2	0	0
IISC	8.0	−0.1	0	−0.1	+67.3	−0.1	−0.1
KARR	7.1	0	0	0	+0.5	+0.6	+0.6
KAT1	5.5	0	0	0	+95.5	+0.2	+0.2
MATE	9.3	0	0	0	+0.1	+0.1	+0.1
MORP	10.1	0	+0.1	+0.1	+0.3	+0.2	+0.2
NICO	7.2	0	0	0	+0.2	0	0
PDEL	8.0	0	−0.1	−0.1	+0.2	+0.3	+0.3
PERT	6.4	+0.1	+0.1	+0.1	+9.7	+0.4	+0.5
PTBB	7.7	0	0	0	+0.2	+0.2	+0.2
QAQ1	6.9	+0.2	0	+0.3	+1.6	+0.4	+0.6
REYK	4.4	0	−0.1	0	+1.0	+0.2	+0.2
SCOR	4.8	0	+0.1	+0.1	+1.4	+0.1	+0.1
THU3	4.9	−0.1	0	−0.1	+95.9	+1.0	+1.0
WTZR	5.8	0	0	0	+0.2	+0.2	+0.2
WUHN	8.3	0	0	−0.1	+0.7	−0.2	−0.2
XMIS	8.6	+0.1	0	+0.1	+92.8	−0.1	−0.1
ZIMM	6.1	0	0	0	+0.3	+0.1	+0.1
Mean	6.60	0	0	0	+17.08	+0.19	+0.20

[a]Without height correction to *aw* and the subsequent wet mapping function

[b]With height correction to *aw* and the subsequent wet mapping function

elevation angles, station heights and orbital altitudes. However, such error does not seem to influence the RMS errors of the retrieved ZTDs presented here.

To further investigate the performance of the VMF1-FC mapping functions, the coordinate estimates are compared against the mean coordinates which are estimated using the VMF1-site dataset (see Fig. 5). In this figure, the Up component, rather than Easting and Northing, is more affected by change of mapping functions. The Up component remains unchanged at stations DAV1 (Davis, Antarctic) and HERS (Hailsham, UK), but deteriorates slightly at station IISC (Bangalore, India) when a height correction to the wet mapping function is applied. The degraded Up component indicates the unsuccessful regression of *aw* at IISC, which is likely caused by the terrain complexity shown in Fig. 1, or by the substantial spatial and temporal variation of water vapor at this tropical station. Overall, its ZTD and coordinate estimates, with and without height corrections to *aw*, agree well with each other. This suggests that any height correction to coefficient *aw* is unnecessary in this scenario. At all these three stations, which are in different climatic zones, the improvement from mapping functions using the VMF1-FC dataset (see VMF1-FC1 solutions) occurs, although this is very minor at stations HERS and IISC.

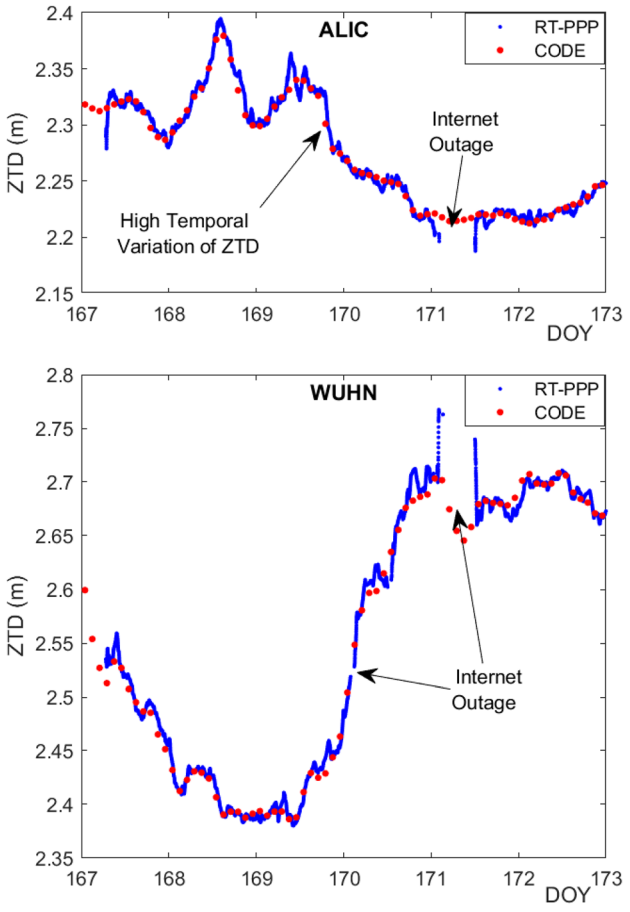

Fig. 4 How high temporal variation of ZTD, minor and major internet outages affect the ZTD retrievals

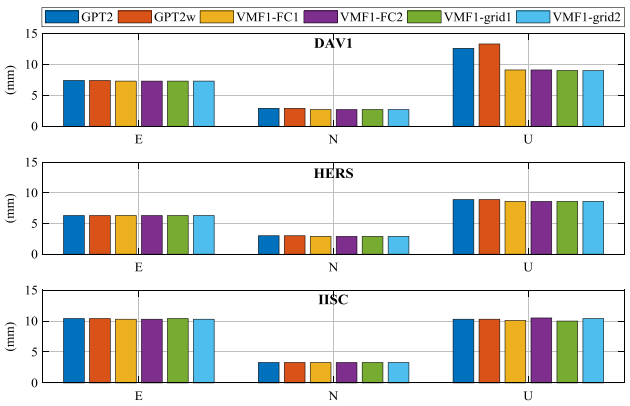

Fig. 5 RMS errors of the three components of station coordinates at stations DAV1 (in polar regions), HERS (in extratropical region) and IISC (in tropical region). In this scenario, the a priori ZHD derived from in situ meteorological data is held constant while different mapping functions are used in PPP

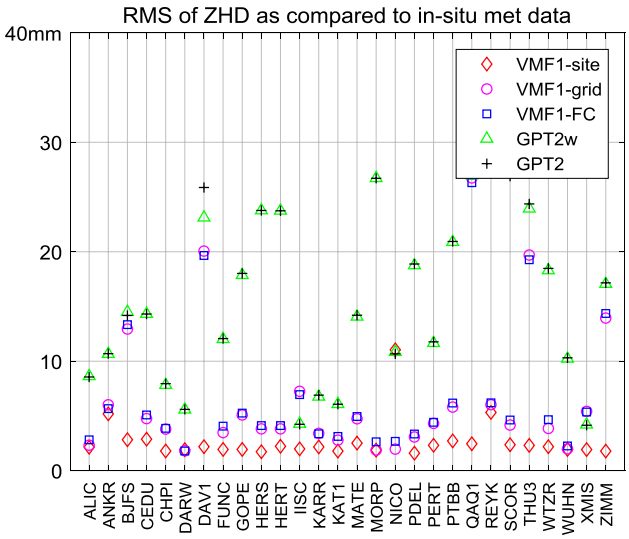

Fig. 6 RMS errors of ZHD derived from various sources as compared to in situ meteorological data in the RINEX format

4 Performance of VMF1-FC ZHD

We also assess the accuracy of ZHD estimates derived from the GPT2, GPT2w, VMF1-FC, VMF1-grid and VMF1-site models using the in situ meteorological data provided in the RINEX format. Figure 6 shows the RMS errors of the ZHD estimates at each of the 28 stations during 2016. The RMS errors are calculated using the epochs when there is in situ meteorological data available. The figure shows that the post-processed VMF1-site is the most accurate among the five models, with ZHD RMS errors <5 mm at most of the selected stations. This is followed by VMF1-grid and VMF1-FC, from which the derived ZHDs are close to each other and the RMS errors are <20 mm. There is one station QAQ1 (Qaqortoq, Greenland) where VMF1-FC does not agree well with the in situ meteorological data. This may be an environmental effect since this station is close to the Arctic. Another potential cause is the terrain complexity, i.e., the station height is 105 m while the four grid heights are 7 m, 328 m, 1817 m and 2554 m. Another two stations, DAV1 in the Antarctic and THU3 in the Arctic, are also with ZHD RMS errors approximately 20 mm.

As expected, the empirical models are coarser in comparison with the routinely updated VMF1 models. Although GPT2w is an update from GPT2, with a higher horizontal resolution of $1°\times1°$ replacing $5°\times5°$, the improvement in terms of ZHD is still very minor.

In real-time PPP, the VMF1-FC mapping functions are held constant to assess the performance of the a priori ZHDs

Table 2 RMS errors of ZTDs using reference ZTD products from CODE. VMF1-FC mapping functions are held constant, while different a priori ZHDs are used in PPP. Columns 3–7 show the differences to VMF1-FC solutions, and a positive value indicates that the corresponding RMS error is larger than its VMF1-FC counterpart

Station	VMF1-FC (RMS:mm)	GPT2 (Δ:mm)	GPT2w (Δ:mm)	VMF1-grid (Δ:mm)	Rinex (Δ:mm)
ALIC	4.7	+0.2	+0.2	0	+0.1
ANKR	5.5	0	0	0	0
BJFS	5.6	+0.4	+0.4	+0.1	+0.1
CEDU	7.5	+0.3	+0.3	0	−0.2
CHPI	6.3	−0.1	−0.1	0	−0.2
DARW	5.6	0	0	0	0
DAV1	3.0	+0.6	+0.5	0	0
FUNC	6.3	0	0	0	0
GOPE	7.0	0	0	0	+0.1
HERS	6.3	0	0	0	−0.1
HERT	8.1	−0.2	−0.1	+0.2	+0.1
IISC	8.1	−0.1	0	−0.1	−0.1
KARR	7.2	0	−0.1	−0.1	−0.1
KAT1	5.5	0	0	0	0
MATE	9.4	−0.2	−0.2	−0.1	−0.1
MORP	10.2	−0.2	−0.2	−0.1	−0.1
NICO	7.1	+0.1	0	0	+0.1
PDEL	8.1	0	0	0	−0.1
PERT	6.4	+0.4	+0.3	−0.1	0
PTBB	7.6	0	0	0	+0.1
QAQ1	6.3	+0.7	+0.6	0	+0.6
REYK	4.5	0	0	0	−0.1
SCOR	4.9	−0.1	−0.1	0	−0.1
THU3	5.0	+0.1	+0.1	0	−0.1
WTZR	5.9	−0.1	−0.1	0	−0.1
WUHN	8.3	+0.2	+0.2	0	0
XMIS	8.6	−0.2	−0.2	0	0
ZIMM	6.1	−0.1	−0.1	0	0
Mean	6.61	+0.06	+0.05	0	0

from various models. Table 2 shows that the performance of GPT2, GPT2w, VMF1-FC, VMF1-grid and in situ meteorological data are quite close, with differences between ZTD RMS errors smaller than 0.4 mm at the 28 stations, except two polar stations DAV1 and QAQ1. Table 2 also shows that if the mapping functions (such as those provided by the VMF1-FC model) are fairly accurate, the estimated ZWDs can compensate to a large extent for the shortcomings of the a priori ZHD model. Further improvement to the a priori ZHD such as those derived from the VMF1-grid and in situ meteorological data brings very minor improvement of the estimation of ZTD. Besides ZTD, the estimated station coordinates are also assessed in this scenario. Figure 7 shows the RMS errors of the station coordinates in three directions. The figure shows that at both stations HERS and IISC, changing of a priori ZHDs brings a very minor change of coordinates in Up direction.

The ZTD retrievals at polar stations DAV1 and QAQ1 show the disadvantage of using the a priori ZHD values (besides the mapping functions as is pointed out in the previous section) derived from models GPT2 and GPT2w. This is probably due to the actual variations not being accounted for by the seasonal GPT pressure values, as was pointed out by Kouba (2009). Fortunately, due to the low variation of water vapor at these two stations, the retrievals of ZTD using the GPT2 ZHD are still successful, with RMS errors of 3.6 mm and 7.0 mm, respectively.

5 Performance of VMF1-FC ZWD

While the GPT2 model only provides ZHD and mapping functions, the GPT2w and VMF1 series models also provide ZWD which can also be used in PPP processing. Table 3 shows the ZTD solutions using different combinations of

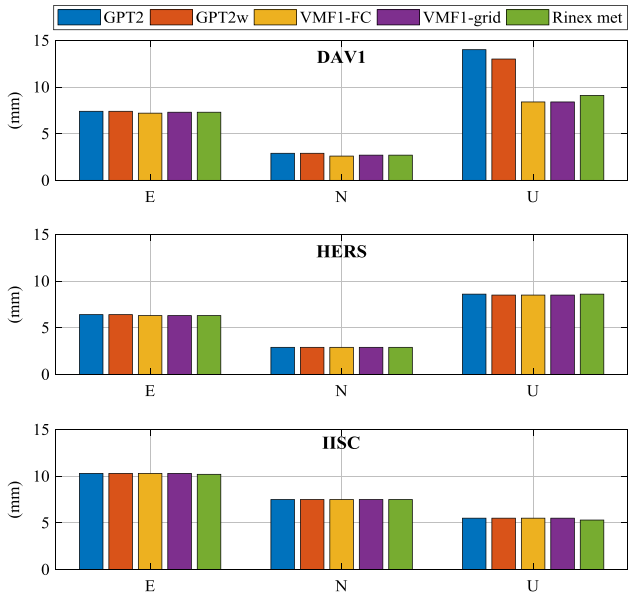

Fig. 7 RMS errors of the three components of station coordinates at stations DAV1 (in polar regions), HERS (in extratropical region) and IISC (in tropical region). In this scenario, VMF1-FC mapping functions are held constant while different a priori ZHDs are used in PPP

tropospheric delay parameters. Column 2 (the *VMF1-FC3 solutions*) shows the ZTD RMS errors using mapping functions, a priori ZHD and ZWD derived from the VMF1-FC dataset. Compared to the solutions without the a priori ZWD from the *VMF1-FC model* (*the VMF1-FC1 solutions*), the RMS errors are reduced substantially at most of the selected stations. The improvement is even more significant in comparison with the solutions using the GPT2 model. This is partly because the GPT2 model is also less accurate in mapping functions and ZHD parameter, which is demonstrated in the previous two sections.

We split the researched 70 days into five sessions with 2 weeks in each session. We then include six two-week sessions, i.e., October 16–30, 2018, for comparison. This is to check the performance of these tropospheric models for real-time PPP in different seasons. The RMS errors in Fig. 8 show that the VMF1-FC model performs consistently better than the empirical models such as GPT2 and GPT2w, and that the RMS errors of the retrieved ZTDs are ≤ 10 mm at each station in different seasons.

The previous sections validate the ZTDs derived from real-time PPP within the GNSS domain. Such ZTDs are also validated using meteorological data from nearby radiosonde stations. The radiosonde data are available from a repository of atmosphere profiles provided by the National Oceanic and Atmospheric Administration (NOAA, https://ruc.noaa.gov/raobs/intl/Data_request.cgi). Meteorological variables of pressure P, temperature T and water vapor partial pressure P_w from the radiosonde profiles are then used to calculate the atmospheric refractivity N which consists of the hydrostatic part N_h and the wet part N_w, using the following equation

$$N = N_h + N_w = k_1 \frac{(P - P_w)}{T} + \left(k_2 \frac{P_w}{T} + k_3 \frac{P_w}{T^2} \right) \tag{9}$$

where $k_1 = 77.6$ [K/hPa], $k_2 = 70.4$ [K/hPa] and $k_3 = 3.739 \times 10^5$ [K2/hPa] are refractivity constants from (Bevis et al. 1994). The ZTD can then be calculated from the integration of refractivity profiles using Eq. (10)

$$\mathrm{ZTD} = 10^{-6} \int_{h_0}^{\infty} \left(N_h(z) + N_w(z) \right) \mathrm{d}z \tag{10}$$

where h_0 is the ellipsoid height of radiosonde station.

Table 4 lists the comparisons between the PPP and the radiosonde ZTDs. One can see that the RMS values look worse when radiosonde data are used instead of the CODE products. This is partly because the IGS and radiosonde stations are not perfectly colocated. When the inter-station distance is within 50 km, the RMS errors are ≤ 15 mm except station WUHN according to this table. However, when the inter-station distance is greater than 50 km, the PPP ZTDs no longer agree well with the reference data. Another factor that makes ZTD comparisons more complex is the station height. The radiosonde measurements are reconstructed to refractivity profiles from the radiosonde heights upward prior to the integration. When the radiosonde height is greater than the IGS height, the radiosonde hydrostatic refractivities are extrapolated downward applying a scale factor for underlying IGS stations to account for the height difference. The wet refractivity is simply assumed to be constant below the radiosonde heights.

In GNSS meteorology, the ZWD is multiplied by a dimensionless proportionality constant and then converted into PWV. For a typical value 0.16 of the constant in a moderate temperature condition (i.e., 20 °C), an error of 15 mm in ZTD or ZWD results in an error of 2.4 mm in the subsequent PWV. This is sufficiently enough for weather nowcasting (De Haan 2006).

The advantage of introducing a priori ZWD into PPP positioning is also confirmed in the RMS errors of the Easting, Northing and Up components in Fig. 9. According to this figure, the improvement in the quality of the estimated coordinates from including a priori ZWD values is

Table 3 RMS errors of ZTDs using reference ZTD products from CODE. Columns 3–11 show the differences to VMF1-FC solutions, and a positive value indicates that the corresponding RMS error is larger than its VMF1-FC counterpart

Station	VMF1-FC3[a] (RMS)	VMF1-FC1[b] (Δ:mm)	VMF1-FC4[c] (Δ:mm)	VMF1-grid1[b] (Δ:mm)	VMF1-grid3[a] (Δ:mm)	VMF1-grid4[c] (Δ:mm)	GPT2 (Δ:mm)	GPT2w1[d] (Δ:mm)	GPT2w2[e] (Δ:mm)
ALIC	4.8	−0.1	0	−0.1	−0.1	−0.1	0	0	0
ANKR	5.4	+0.1	0	+0.2	−0.1	−0.1	+0.4	+0.3	+0.3
BJFS	5.5	+0.1	+0.1	+0.2	0	0	+0.3	+0.2	+0.2
CEDU	6.6	+0.9	+0.2	+0.9	0	0	+0.8	+0.7	+0.8
CHPI	5.8	+0.5	0	+0.5	+0.1	+0.1	+0.4	+0.4	+0.4
DARW	5.3	+0.3	0	+0.3	+0.1	+0.1	+0.3	+0.3	+0.3
DAV1	3.0	0	0	0	0	0	+1.3	+1.2	+1.2
FUNC	6.1	+0.2	0	+0.2	+0.1	+0.1	+0.3	+0.3	+0.3
GOPE	7.1	−0.1	0	−0.1	−0.1	−0.1	+0.2	+0.2	+0.2
HERS	6.0	+0.3	0	+0.2	+0.1	+0.1	+0.8	+0.8	+0.8
HERT	8.2	−0.1	0	0	−0.2	−0.2	−0.1	−0.2	−0.2
IISC	7.6	+0.5	+0.1	+0.4	+0.3	+0.3	+0.4	+0.4	+0.4
KARR	7.4	−0.2	0	−0.3	+0.5	+0.5	+0.3	+0.4	+0.4
KAT1	5.5	0	0	0	−0.1	0	+0.2	+0.2	+0.2
MATE	8.9	+0.5	0	+0.5	+0.1	+0.1	+0.3	+0.3	+0.3
MORP	9.6	+0.6	+0.1	+0.6	−0.6	−0.6	+0.6	+0.6	+0.6
NICO	7.4	−0.3	0	−0.3	0	0	−0.3	−0.2	−0.2
PDEL	8.4	−0.3	0	−0.3	−0.1	−0.1	0	0	0
PERT	6.6	−0.2	−0.1	−0.2	−0.1	−0.1	+0.8	+0.8	+0.8
PTBB	6.8	+0.8	0	+0.8	+0.2	+0.2	+0.9	+0.9	+1.0
QAQ1	6.3	0	0	0	+0.1	+0.1	+1.1	+1.2	+1.2
REYK	4.6	−0.1	0	−0.1	0	0	+0.1	+0.1	+0.1
SCOR	4.8	+0.1	0	+0.1	+0.1	+0.1	0	0	0
THU3	4.8	+0.2	0	+0.3	−0.1	−0.1	+1.4	+1.4	+1.4
WTZR	5.0	+0.9	0	+0.9	+0.3	+0.3	+1.0	+1.0	+1.0
WUHN	8.2	+0.1	0	+0.1	+0.2	+0.2	+0.1	0	0
XMIS	8.9	−0.3	0	−0.4	+0.3	+0.3	−0.6	−0.6	−0.6
ZIMM	6.1	0	0	0	+0.2	+0.2	+0.1	+0.2	+0.2
Mean	6.45	+0.16	+0.01	+0.16	+0.04	+0.05	+0.40	+0.39	+0.40

[a]With VMF1 mapping functions, a priori ZHD and ZWD; without height correction to ZWD

[b]With VMF1 mapping functions and a priori ZHD; without a priori ZWD

[c]With VMF1 mapping functions, a priori ZHD and ZWD; with height correction to ZWD

[d]With GPT2w mapping functions, a priori ZHD, without a priori ZWD

[e]With GPT2w mapping functions, a priori ZHD and ZWD

particularly significant at stations DAV1 and IISC. RMS errors in the Up component are reduced by 10.8 mm (19.2–8.4) and 3.5 mm (10.3–6.8), respectively, when the VMF1-FC dataset is used instead of the GPT2 model.

The VMF1-FC4 solutions in Table 3, in which ZWD height corrections are accounted for using linear regression, do not show improvement compared to those without height correction (*the VMF1-FC3 solutions*). A further investigation shows that the introduced height correction component of ZWD, which can be up to 50 mm (see Fig. 10), is fully absorbed into the ZWD estimate (an unknown parameter to be estimated in PPP data processing). In other words, the estimated ZWDs can compensate to a large extent for the shortcomings of the a priori ZWD model. This occurs when

Fig. 8 RMS errors of ZTDs with different tropospheric models implemented in PPP over six two-week sessions. Sessions 1–5 are in June 15 to August 24, 2016, while session 6 is October 16–30, 2018

mapping functions and a priori ZHD are held constant. In that case, the ZTD, which is the sum of the a priori ZHD, ZWD and the estimated correction to the a priori ZWD, is not affected. The subsequent height component of the station coordinates, which is highly correlated with the ZWD estimate, also remains unchanged.

6 Conclusions

This research assesses the performance of the VMF1-FC model in terms of its ZHD, ZWD and mapping functions. This model is shown to be superior to the widely used empirical models, such as the NMF (for providing mapping functions), GPT2 (for providing ZHD and mapping functions) and GPT2w in terms of all three components. This result is based on the test at 28 global IGS stations over a 70-day period. It is recommended that the VMF1-FC model be implemented instead of empirical models in real-time applications. Particularly in polar regions, the RMS errors of the retrieved ZTDs can be reduced by 1 mm (stations DAV1, QAQ1 and THU3 in Table 3) if VMF1-FC instead of GPT2 or GPT2w is used. The RMS errors of the position in vertical direction can be reduced from 19.2 mm to 8.4 mm at station DAV1 (Fig. 9). More accurate positions and velocities from GNSS are critical to studies such as sea level rise and glacial isostatic adjustment in polar regions (King et al. 2010).

Moreover, when the VMF1-FC model is implemented, height corrections are essential for the hydrostatic mapping function and ZHD coefficients. However, no established approaches are readily available to account for the wet mapping function and ZWD. This is partly because the wet parameters deviate significantly and are difficult to predict (Boehm et al. 2007). The linear regression method applied in this research is likely affected by this factor. Another potential factor is the terrain complexity around the station as height difference between station height and grid heights can be as large as 1000 m. A horizontal resolution of VMF1-FC dataset higher than the current

Table 4 RMS errors of PPP ZTDs using reference data from nearby radiosonde stations during June 15 to August 24, 2016. IGS stations are grouped in terms of the surface distances in kilometers between the IGS and radiosonde stations. Three stations CHPI, THU3 and XMIS do not have radiosonde data for comparison during the research period

IGS station	Surface Dist. (km)	IGS Ht (m)	Radiosonde Ht (m)	ZTD RMS (mm)
ALIC	15	588	541	5.5
ANKR	12	950	894	13.7
BJFS	49	104	55	15.0
CEDU	31	152	22	4.0
CHPI	24	627	537	–
DAV1	1	26	13	13.6
FUNC	2	35	56	11.6
GOPE	26	554	303	12.0
HERS	4	27	54	10.1
HERT	4	27	54	10.9
IISC	6	931	921	14.4
MORP	25	95	141	9.9
NICO	1	167	161	12.8
PERT	15	48	29	9.7
REYK	37	32	54	8.7
SCOR	1	74	66	9.2
THU3	2	24	77	–
WUHN	24	41	23	32.2
ZIMM	40	913	490	11.4
DARW	57	77	30	15.3
PTBB	68	90	69	13.7
QAQ1	61	66	4	17.2
WTZR	78	626	419	14.8
KARR	172	120	6	21.6
KAT1	260	139	30	36.9
MATE	105	495	10	23.4
PDEL	164	61	113	24.2
XMIS	443	271	366	–

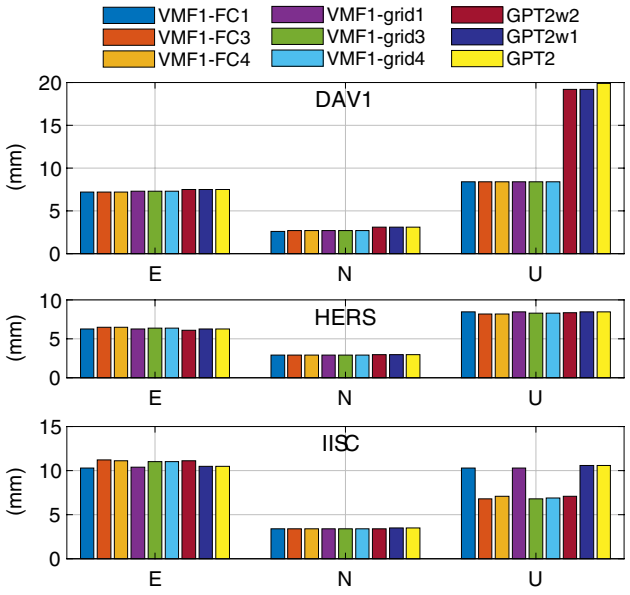

Fig. 9 RMS errors of the three components of station coordinates at stations DAV1 (in polar regions), HERS (in extratropical region) and IISC (in tropical region). In this scenario, VMF1-FC mapping functions are held constant while different a priori ZHDs are used in PPP

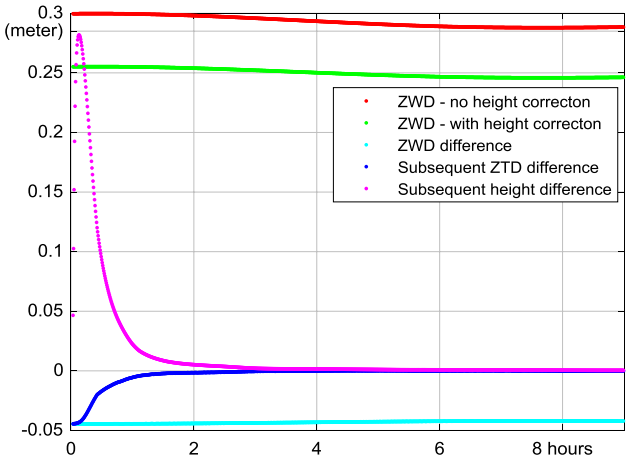

Fig. 10 Changing of ZTD and height estimated from PPP at station IISC when different a priori ZWDs are used

2.5° × 2.0° will solve this. Fortunately, the PPP solutions with and without height corrections for these two wet coefficients show very minor differences not just in ZTD estimates, but also in the three coordinate components at most of the selected stations. This research shows that when VMF1-FC mapping functions are applied, the ZWD estimates in PPP can compensate for the shortcomings of the a priori ZHD and ZWD models to a large extent. In this case, it is recommended using the values at zero height for *aw* (and the subsequent wet mapping function) and the value at the mean grid height for ZWD at any geographic locations.

This research confirms that PPP is a reliable approach to retrieve ZTD in real time. The ZTD solutions agree well with the reference ZTD products, and the RMS errors at 27 out of the 28 stations are < 10 mm with reference to the CODE products, even when GPT2 and GPT2w are used for the tropospheric delay modeling. Only at station MORP, the RMS error reaches 10.2 mm as shown in Table 3. This easily meets the accuracy requirements if they are included into NWP models (De Haan 2006). Currently, empirical models dominate real-time GNSS positioning, while the ever-increasing predictive capabilities of NWP models are still underutilized to enhance the real-time applications. More and more such applications as incorporating forecast NWP datasets (Lu et al. 2017; Wilgan et al. 2017) are foreseen in the near future.

Acknowledgements The authors would like to thank BKG for providing the original BNC software package and real-time corrections, the Vienna University of Technology for providing the VMF1 datasets (http://ggosatm.hg.tuwien.ac.at/DELAY/), the NOAA for providing the radiosonde dataset (https://ruc.noaa.gov/raobs/intl/Data_request.cgi), CODE for providing the ZTD products (http://ftp.aiub.unibe.ch/CODE/) and IGS (Dow et al. 2009) for providing the real-time corrections.

References

Agrotis L, Caissy M, Weber G, Ge M, MacLeod K, Hernández-Pajares M (2012) IGS real time infrastructure: from pilot project to operational service. Paper presented at the PPP-RTK and Open Standards Symposium, Frankfurt, Germany, 12–13 March

Bevis M, Businger S, Herring TA, Rocken C, Anthes RA, Ware RH (1992) GPS meteorology: remote sensing of atmospheric water vapor using the global positioning system. J Geophys Res 97:15,787–715,801. https://doi.org/10.1029/92jd01517

Bevis M, Businger S, Chiswell S, Herring TA, Anthes RA, Rocken C, Ware RH (1994) GPS meteorology: mapping zenith wet delays onto precipitable water. J Appl Meteorol 33:379–386. https://doi.org/10.1175/1520-0450(1994)033%3c0379:GMMZWD%3e2.0.CO;2

Bevis M, Chiswell S, Businger S, Herring TA, Bock Y (1996) Estimating wet delays using numerical weather analyses and predictions. Radio Sci 31:477–487. https://doi.org/10.1029/96RS00008

Boehm J, Niell A, Tregoning P, Schuh H (2006a) Global Mapping Function (GMF): a new empirical mapping function based on numerical weather model data. Geophys Res Lett 33:7. https://doi.org/10.1029/2005gl025546

Boehm J, Werl B, Schuh H (2006b) Troposphere mapping functions for GPS and very long baseline interferometry from European Centre for Medium-Range Weather Forecasts operational analysis data. J Geophys Res B Solid Earth 111:B02406. https://doi.org/10.1029/2005JB003629

Boehm J, Heinkelmann R, Schuh H (2007) Short note: a global model of pressure and temperature for geodetic applications. J Geodesy 81:679–683. https://doi.org/10.1007/s00190-007-0135-3

Boehm J, Kouba J, Schuh H (2009) Forecast Vienna mapping functions 1 for real-time analysis of space geodetic observations. J Geodesy 83:397–401. https://doi.org/10.1007/s00190-008-0216-y

Boehm J, Moeller G, Schindelegger M, Pain G, Weber R (2015) Development of an improved empirical model for slant delays in the troposphere (GPT2w). GPS Solut 19:433–441. https://doi.org/10.1007/s10291-014-0403-7

Dach R et al (2009) GNSS processing at CODE: status report. J Geodesy 83:353–365. https://doi.org/10.1007/s00190-008-0281-2

Davis JL, Herring TA, Shapiro II, Rogers AEE, Elgered G (1985) Geodesy by radio interferometry effects of atmospheric modeling errors on estimates of baseline length. Radio Sci 20:1593–1607. https://doi.org/10.1029/RS020i006p01593

De Haan S (2006) National/regional operational procedures of GPS water vapour networks and agreed international procedures. World Meteorological Organization, KNMI, De Bilt

Dousa J, Elias M (2014) An improved model for calculating tropospheric wet delay. Geophys Res Lett 41:4389–4397. https://doi.org/10.1002/2014GL060271

Dow JM, Neilan RE, Rizos C (2009) The International GNSS Service in a changing landscape of Global Navigation Satellite Systems. J Geodesy 83:191–198. https://doi.org/10.1007/s00190-008-0300-3

Fund F, Morel L, Mocquet A, Boehm J (2011) Assessment of ECMWF-derived tropospheric delay models within the EUREF Permanent Network. GPS Solut 15:39–48. https://doi.org/10.1007/s10291-010-0166-8

Herring TA (1992) Modelling atmospheric delays in the analysis of space geodetic data. In: DeMunkand JC, Spoelstra TA (eds) Symposium on refraction of transatmospheric signals in geodesy. Netherlands Geodetic Commission, Delft, pp 157–164

King MA, Altamimi Z, Boehm J, Bos M, Dach R, Elosegui P et al (2010) Improved constraints to models of glacial isostatic adjustment: a review of the contribution of ground-based geodetic observations. Surv Geophys 31(5):465–507. https://doi.org/10.1007/s10712-010-9100-4

Kouba J (2008) Implementation and testing of the gridded Vienna mapping function 1 (VMF1). J Geodesy 82:193–205. https://doi.org/10.1007/s00190-007-0170-0

Kouba J (2009) Testing of global pressure/temperature (GPT) model and global mapping function (GMF) in GPS analyses. J Geodesy 83:199–208. https://doi.org/10.1007/s00190-008-0229-6

Kouba J, Heroux P (2001) Precise point positioning using IGS orbit and clock products. GPS Solut 5:12–28. https://doi.org/10.1007/PL00012883

Lagler K, Schindelegger M, Böhm J, Krásná H, Nilsson T (2013) GPT2: empirical slant delay model for radio space geodetic techniques. Geophys Res Lett 40:1069–1073. https://doi.org/10.1002/grl.50288

Lu C, Li X, Zus F, Heinkelmann R, Dick G, Ge M, Wickert J, Schuh H (2017) Improving BeiDou real-time precise point positioning with numerical weather models. J Geodesy 91:1019–1029. https://doi.org/10.1007/s00190-017-1005-2

Marini JW (1972) Correction of satellite tracking data for an arbitrary tropospheric profile. Radio Sci 7:223–231. https://doi.org/10.1029/RS007i002p00223

Mervart L, Weber G (2013) BKG ntrip client (BNC) version 2.8. BKG, Frankfurt

Niell AE (1996) Global mapping functions for the atmosphere delay at radio wavelengths. J Geophys Res B Solid Earth 101:3227–3246. https://doi.org/10.1029/95JB03048

Petit G, Luzum B (2010) Chapte 7: Displacement of reference points. In: Petit G, Luzum B (eds) IERS technical note No. 36 (IERS conventions 2010)

Tregoning P, Boers R, O'Brien D, Hendy M (1998) Accuracy of absolute precipitable water vapor estimates from GPS observations. J Geophys Res D Atmos 103:28701–28710. https://doi.org/10.1029/98JD02516

Wilgan K, Hadas T, Hordyniec P, Bosy J (2017) Real-time precise point positioning augmented with high-resolution numerical weather prediction model. GPS Solut 21:1341–1353. https://doi.org/10.1007/s10291-017-0617-6

Yuan Y (2015) Real-time retrieval of precipitable water vapour from GNSS precise point positioning. Ph.D., RMIT University

Yuan Y, Zhang K, Rohm W, Choy S, Norman R, Wang C-S (2014) Real-time retrieval of precipitable water vapor from GPS precise point positioning. J Geophys Res Atmos 119:2014JD021486. https://doi.org/10.1002/2014jd021486

Zumberge JF, Heflin MB, Jefferson DC, Watkins MM, Webb FH (1997) Precise point positioning for the efficient and robust analysis of GPS data from large networks. J Geophys Res B Solid Earth 102:5005–5017. https://doi.org/10.1029/96JB03860

Zus F, Dick G, Dousa J, Wickert J (2015) Systematic errors of mapping functions which are based on the VMF1 concept. GPS Solut 19:277–286. https://doi.org/10.1007/s10291-014-0386-4